CHEMISTRY OF MATERIALS
Article

Chem. Mater. **2010,** *22,* 101–107 101
DOI:10.1021/cm9029566

Nanostructured $CaCO_3$ Thin Films Formed on the Urease Multilayers Prepared by the Layer-by-Layer Deposition

Bongjun Yeom and Kookheon Char*

Center for Functional Polymer Thin Films, School of Chemical and Biological Engineering, The WCU Program of Chemical Convergence for Energy and Environment, Seoul National University, Seoul, 151-744, Korea

Received September 23, 2009. Revised Manuscript Received November 14, 2009

Nanostructured $CaCO_3$ (NCC) thin films with honeycomb-shaped nanopores were obtained at the surface of urease-embedded multilayers prepared by the layer-by-layer deposition. Amorphous $CaCO_3$ (ACC) droplets were initially nucleated from the multilayer surface, because of the enzymatic reaction of ureases to produce CO_2, particularly when the saturation index of $CaCO_3$ in the crystal-forming solution is above 1.89 based on the calcite saturation. Once ACC droplets successfully covered the entire surface of the urease multilayers, the ACC layers underwent the transformation into the crystalline {104}-faceted nanostructured calcite thin films with square pores, ~30 nm on each side, in a humidity-controlled chamber. Furthermore, such NCC thin films were realized on various substrates (two-dimensional patterns, PS microspheres, and sawtooth-shaped three-dimensional patterns) taking full advantage of the conformal multilayer coating capability of the layer-by-layer deposition.

Introduction

Inspired by the biomineralization processes abundant in living organisms, studies on biomimicry have received significant attention in recent years.[1,2] Particularly, keen focus has been placed on biominerals such as coccospheres of coccolithophorids, skeletons of sea urchin, and nacres of abalone shells, because of their unique optical and superior mechanical properties derived from the hierarchical structures involving calcium carbonate crystals coupled with a small fraction of organic moieties.[3,4] Undoubtedly, there have been numerous efforts to understand the biomineralization process to mimic the delicate structure of biominerals existing in nature toward the novel design of inorganic/organic nanocomposites. Also, nanoscale manipulation of biominerals has been intensively studied to control their shape, size, and orientation, which would play a critical role in determining their unique functionality.[5−11] Because of the advantages such as environmental benignity and high performance with low-cost processing, calcium-containing biominerals have emerged as one of potential candidates for various applications such as cell culture, drug delivery, tissue engineering, micro/nanocomposites, and biocompatible organs.[5,6]

To mimic the complex organic/inorganic nanohybrid structures containing $CaCO_3$ crystals such as nacres, many researchers have studied the $CaCO_3$ crystal growth on organic substrates with ordered structures in nano/micro dimension.[7−18] Meldrum et al. reported the $CaCO_3$ growth on a micrometer-sized complex structured mold by the double-sided diffusion method, placing the mold between tubes containing both Ca^{2+} and CO_3^{2-} solutions.[19,20] Qi and co-workers used highly supersaturated solution to realize the three-dimensionally ordered microstructure.[21] Gower et al. also prepared $CaCO_3$ thin films on the patterned self-assembled

*Author to whom correspondence should be addressed. E-mail: khchar@plaza.snu.ac.kr.

(1) Mann, S.; Webb, J.; Williams, R. J. P. *Biomineralization: Chemical and Biochemical Perspectives*; VCH Publishers: New York, 1989.
(2) Weiner, S.; Addadi, L. *J. Mater. Chem.* **1997**, *7*(5), 689.
(3) Politi, Y.; Arad, T.; Klein, E.; Weiner, S.; Addadi, L. *Science* **2004**, *306*(5699), 1161.
(4) Sanchez, C.; Arribart, H.; Guille, M. M. G. *Nat. Mater.* **2005**, *4*(4), 277.
(5) Wang, C. Y.; He, C. Y.; Tong, Z.; Liu, X. X.; Ren, B. Y.; Zeng, F. *Int. J. Pharm.* **2006**, *308*(1−2), 160.
(6) Popescu, D. C.; van Leeuwen, E. N. M.; Rossi, N. A. A.; Holder, S. J.; Jansen, J. A.; Sommerdijk, N. *Angew. Chem., Int. Ed.* **2006**, *45* (11), 1762.
(7) Lu, C. H.; Qi, L. M.; Cong, H. L.; Wang, X. Y.; Yang, J. H.; Yang, L. L.; Zhang, D. Y.; Ma, J. M.; Cao, W. X. *Chem. Mater.* **2005**, *17* (20), 5218.
(8) Ludwigs, S.; Steiner, U.; Kulak, A. N.; Lam, R.; Meldrum, F. C. *Adv. Mater.* **2006**, *18*(17), 2270.
(9) Aizenberg, J.; Muller, D. A.; Grazul, J. L.; Hamann, D. R. *Science* **2003**, *299*(5610), 1205.
(10) Wei, H.; Ma, N.; Shi, F.; Wang, Z. Q.; Zhang, X. *Chem. Mater.* **2007**, *19*(8), 1974.
(11) Kato, T.; Sugawara, A.; Hosoda, N. *Adv. Mater.* **2002**, *14*(12), 869.
(12) Zhang, S. K.; Gonsalves, K. E. *Langmuir* **1998**, *14*(23), 6761.
(13) Hosoda, N.; Kato, T. *Chem. Mater.* **2001**, *13*(2), 688.
(14) Sakamoto, T.; Oichi, A.; Nishimura, T.; Sugawara, A.; Kato, T. *Polym. J.* **2009**, *41*(7), 522.
(15) Gower, L. B.; Odom, D. J. *J. Cryst. Growth* **2000**, *210*(4), 719.
(16) Naka, K.; Chujo, Y. *Chem. Mater.* **2001**, *13*(10), 3245.
(17) Litvin, A. L.; Valiyaveettil, S.; Kaplan, D. L.; Mann, S. *Adv. Mater.* **1997**, *9*(2), 124.
(18) Amos, F. F.; Sharbaugh, D. M.; Talham, D. R.; Gower, L. B.; Fricke, M.; Volkmer, D. *Langmuir* **2007**, *23*(4), 1988.
(19) Park, R. J.; Meldrum, F. C. *Adv. Mater.* **2002**, *14*(16), 1167.
(20) Loste, E.; Park, R. J.; Warren, J.; Meldrum, F. C. *Adv. Funct. Mater.* **2004**, *14*(12), 1211.
(21) Li, C.; Qi, L. M. *Angew. Chem., Int. Ed.* **2008**, *47*(13), 2388.

Published on Web 12/07/2009

monolayer surfaces.[22] However, it still remains as a daunting task to realize the biomimetic $CaCO_3$/organic hybrid structure, in view of large area fabrication and the conformal hybrid coating on complex microstructures involving curved surface. The difficulty in the formation of $CaCO_3$ crystals is mainly due to the problems associated with the diffusion of source materials in confined geometry as well as with the disturbance by the faceted growth of crystals on highly curved substrates. To overcome these hurdles, in vitro synthesis of amorphous calcium carbonate (ACC) has been reported, because naturally formed ACCs were regarded as a key material to explain the biomineralization process.[23−28] Because the ACC exists only in the amorphous state, it is more likely to form the ACC on complex micropatterns compared with other crystalline polymorphs such as calcite, vaterite, and aragonite. However, the ACC is inherently unstable in an ambient environment; the detailed characteristics of the ACC have not been fully understood yet.[29,30]

The layer-by-layer deposition is a versatile route to prepare multilayered functional polymer thin films, employing the adsorption driving forces such as electrostatic interaction, hydrogen bonding, and many other chemical/physical interactions for adsorbing pairs.[31−34] Enzymes and biopolymers can also be immobilized within the multilayered thin films to express programmed functions to be used in applications such as enzymatic reactors and chemical sensors.[35,36] Recently, urease, which is classified as one type of enzymes, has been used to generate carbonate ions for the synthesis of $CaCO_3$ crystals, as a result from the hydrolytic decomposition of urea by the enzymatic reaction.[37−39] It has been reported that immobilized urease was used to fill the void space in hollow microtubules with $CaCO_3$, as well as to form $CaCO_3$ bulk particles at the exterior surface of fibers.[40−42]

In the present study, we suggest a novel method to fabricate nanostructured $CaCO_3$ (NCC) thin films based on the enzymatic reaction of urease immobilized within a multilayer film, which is prepared by the layer-by-layer deposition. Amorphous $CaCO_3$ (ACC) droplets are initially formed from the multilayer surface and those droplets then grow and merge with other ACC droplets to fill the large surface area under the controlled experimental conditions. Subsequently, the ACC thin films transform to {104}-faceted nanostructured crystalline thin films under specific humidity. We have also shown that the NCC thin films can be prepared on various types of synthetic substrates, taking full advantage of the conformal coating capability of the layer-by-layer deposition: NCC thin films are realized in two-dimensional line patterns, on polystyrene microspheres, and also on sawtooth-shaped micropatterns.

Experimental Section

Materials. Poly(diallyldimethylammonium chloride) (abbreviated as PDAC) (M_w = 100 000−200 000), poly(sodium 4-styrenesulfonate) (abbreviated as PSS) (M_w = 70 000), urease (abbreviated as Ur, from jack bean), urea (99+%), $CaCl_2 \cdot 2H_2O$ (99+%), and tris(hydroxylmethyl)aminomethane)) (ultrapure grade) were used as received from Sigma−Aldrich.

Preparation of Ur Multilayers. Silicon wafers were initially cleaned by the treatment with piranha solution (H_2SO_4/H_2O_2 = 7/3 (v/v%)) for 20 min and the surfaces were subsequently negatively charged by heating at 60 °C for 15 min in a mixture of $H_2O/H_2O_2/NH_3$ = 5/1/1 (v/v%), followed by washing in water and drying with a gentle stream of nitrogen. To reduce the substrate effect, PDAC/PSS/PDAC layers were initially deposited on the substrate. First, a silicon substrate was dipped into PDAC solution (1 mg/mL with 0.5 M NaCl) for 10 min, followed by dipping in neutral water for 1 min 2 times. After blowing out excess water on the surface by a gentle stream of nitrogen, the PDAC-covered substrate was dipped into PSS solution (1 mg/mL with 0.5 M NaCl). After the same washing and blowing steps, the substrate was covered with PDAC/PSS layers. After a PDAC layer was subsequently coated, the PDAC/PSS/PDAC coated Si wafer was used as a substrate for the deposition of Ur multilayers. Ur multilayers were prepared on the sublayer coated Si wafer using urease solution (1 mg/mL, pH 8.5 with tris buffer, anionic polyelectrolyte) and PDAC solution (1 mg/mL, pH 8.5 with tris buffer, cationic polyelectrolyte). Also, pH 8.5 buffer solution was used in washing steps. The Ur multilayers ($(Ur/PDAC)_{n+(1/2)}$) were prepared until a desired number of Ur layers ($n + 1$) was obtained. (The value 1/2 in the subscript implies that the top surface of the multilayer is covered with the Ur layer.)

Preparation of ACC Thin Films and Their Phase Transformation. The Ur multilayer film was placed upside down at the air/water interface of $CaCl_2$ solution to suppress the gravitational precipitation of $CaCO_3$ particles on the substrate. The solution contains 0.5 M $CaCl_2 \cdot 2H_2O$ for the source of calcium and 0.5 M urea for the source of carbonate ions. A small amount of $NaHCO_3$ (10 mM) was also added to make the solution supersaturated by $CaCO_3$.

(22) Kim, Y. Y.; Douglas, E. P.; Gower, L. B. *Langmuir* **2007**, *23*(9), 4862.
(23) Addadi, L.; Raz, S.; Weiner, S. *Adv. Mater.* **2003**, *15*(12), 959.
(24) Xu, X. R.; Han, J. T.; Cho, K. *Chem. Mater.* **2004**, *16*(9), 1740.
(25) Faatz, M.; Grohn, F.; Wegner, G. *Adv. Mater.* **2004**, *16*(12), 996.
(26) Addadi, L.; Joester, D.; Nudelman, F.; Weiner, S. *Chem.—Eur. J.* **2006**, *12*(4), 981.
(27) Lee, J. R. I.; Han, T. Y. J.; Willey, T. M.; Wang, D.; Meulenberg, R. W.; Nilsson, J.; Dove, P. M.; Terminello, L. J.; van Buuren, T.; De Yoreo, J. J. *J. Am. Chem. Soc.* **2007**, *129*(34), 10370.
(28) Han, T. Y. J.; Aizenberg, J. *Chem. Mater.* **2008**, *20*(3), 1064.
(29) Ajikumar, P. K.; Wong, L. G.; Subramanyam, G.; Lakshminarayanan, R.; Valiyaveettil, S. *Cryst. Growth Des.* **2005**, *5*(3), 1129.
(30) Huang, S. C.; Naka, K.; Chujo, Y. *Langmuir* **2007**, *23*(24), 12086.
(31) Decher, G. *Science* **1997**, *277*(5330), 1232.
(32) Tang, Z. Y.; Wang, Y.; Podsiadlo, P.; Kotov, N. A. *Adv. Mater.* **2006**, *18*(24), 3203.
(33) Fan, X. W.; Park, M. K.; Xia, C. J.; Advincula, R. *J. Mater. Res.* **2002**, *17*(7), 1622.
(34) Krogman, K. C.; Lowery, J. L.; Zacharia, N. S.; Rutledge, G. C.; Hammond, P. T. *Nat. Mater.* **2009**, *8*(6), 512.
(35) Lvov, Y.; Caruso, F. *Anal. Chem.* **2001**, *73*(17), 4212.
(36) Disawal, S.; Qiu, H. H.; Elmore, B. B.; Lvov, Y. M. *Colloids Surf., B* **2003**, *32*(2), 145.
(37) Sondi, I.; Matijevic, E. *J. Colloid Interface Sci.* **2001**, *238*(1), 208.
(38) Yu, A. M.; Gentle, I.; Lu, G. Q.; Caruso, F. *Chem. Commun.* **2006**, *20*, 2150.
(39) Antipov, A.; Shchukin, D.; Fedutik, Y.; Zanaveskina, I.; Klechkovskaya, V.; Sukhorukov, G.; Mohwald, H. *Macromol. Rapid Commun.* **2003**, *24*(3), 274.
(40) de la Rica, R.; Matsui, H. *Angew. Chem., Int. Ed.* **2008**, *47*(29), 5415.
(41) Xing, Q.; Eadula, S. R.; Lvov, Y. M. *Biomacromolecules* **2007**, *8*(6), 1987.
(42) Shchukin, D. G.; Sukhorukov, G. B.; Price, R. R.; Lvov, Y. M. *Small* **2005**, *1*(5), 510.

After a desired deposition time, the substrate was washed with ethanol, followed by drying in N_2 stream. The ACC thin film formed on a Ur multilayer was immediately placed in a humidity-controlled chamber to induce the phase transformation into nanocrystals.

Fabrication of 2-D and 3-D NCC Film Structures. To realize two-dimensional patterns, a silicon wafer coated with photoresist patterns was used as a substrate for the Ur multilayer deposition. A silicon wafer was first cleaned by a piranha treatment, followed by the coating with hexamethyldisilazane (HMDS) to enhance the adhesion with the photoresist. A photoresist film (AZ1512) spun on the HMDS-coated substrate was baked at 95 °C for 30 min and then exposed to UV light through a photomask. The wafer was developed by an AZ developer, yielding two-dimensional photoresist patterns on a silicon substrate. The entire substrate surface, including the patterned photoresist, was coated with Ur multilayers by the layer-by-layer deposition and an ACC thin film was grown on the entire surface, as described previously. The substrate was then immersed in acetone with ultrasonication for 1 min in order to lift off the photoresist patterns. This procedure results in the ACC thin film grown on top of a Ur multilayer in a selective region that is the opposite site of photoresist patterns. The patterned ACC thin films were then transferred to a humidity chamber, to convert the ACC thin films into NCC thin films. For three-dimensional structures, PS microspheres were initially deposited on a PS petridish by sedimentation, followed by gentle washing step to remove weakly bound beads. A PS petri dish that contained PS microspheres was used as the substrate for Ur multilayer deposition. The preparation for the sawtooth-shaped polyurethane substrate is described elsewhere.[43]

Characterization. Ellipsometric thickness measurements were performed with a ellipsometer (Model L2W15S830, Gaertner Scientific Corp.) with a 632.8-nm He−Ne laser-light source. Optical microscope measurements were performed using a Nikon OPTIPHOT2-POL in reflection mode. Atomic force microscopy (AFM) measurements were performed using a Nanoscope IIIa System (Digital Instruments, Inc.) operating in the tapping mode. Field-emission scanning electron microscope (FE-SEM) images were obtained with a JEOL Model 7401F system after 4 nm of platinum sputtering. X-ray diffraction (XRD) data were obtained with a Bruker powder X-ray diffractometer. Fourier transform infrared (FT-IR) spectra were obtained in transmission mode using a Nicolet Series II Magna-IR System 750 apparatus with a spectral resolution of 4 cm^{-1}. The X-ray photoelectron spectroscopy (XPS) result was obtained with AXIS (KRATOS Corp.)

Results and Discussion

The multilayer thin films ($(Ur/PDAC)_{n+(1/2)}$) containing immobilized urease (Ur) were first prepared by the alternative adsorption of Ur (negatively charged) and poly(diallyldimethylammonium chloride) (PDAC; positively charged strong polyelectrolyte) until a desired amount of Ur was incorporated into the multilayer film (see Figure 1a). The urease content incorporated into the Ur-multilayered thin films was investigated with FT-IR measurements, showing the linear growth in urease content and the enzymatic activity of the urease multilayers

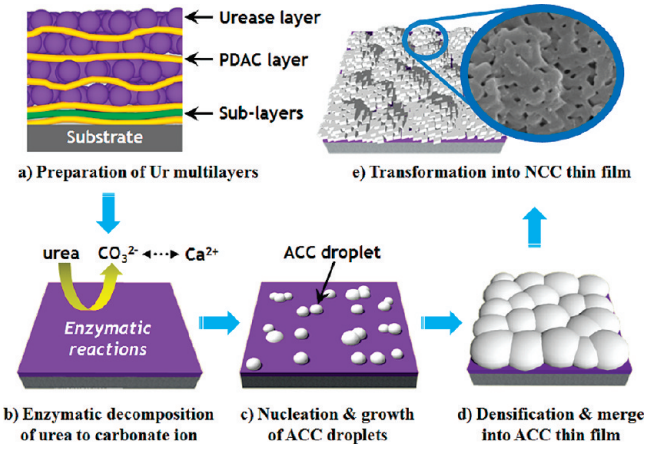

Figure 1. Schematic illustration for the preparation of a nanostructured $CaCO_3$ (NCC) thin film on a urease-containing multilayer.

was also monitored by the colorimetric assay using a pH-sensitive dye reported elsewhere, demonstrating the good agreement between enzymatic activity and FT-IR measurements.[35] (See Figure S1 in the Supporting Information.) A Ur multilayer ($(Ur/PDAC)_{6+(1/2)}$) that contained seven layers of Ur was selected for the formation and crystallization of $CaCO_3$ in this study and the film thickness of the Ur multilayer was determined to be ~50 nm. A silicon wafer containing the Ur multilayered film was then turned upside down and placed onto a solution containing $CaCl_2 \cdot 2H_2O$, urea, and $NaHCO_3$ to initiate the growth of $CaCO_3$ from the multilayer surface (see Figures 1c and 1d).

To investigate the formation of amorphous $CaCO_3$ (ACC) on the Ur-containing multilayer surface in detail, a series of evolving surface morphologies, taken using field-emission scanning electron microscopy (FE-SEM), were collected as a function of growth (or treatment) time. Before the onset of $CaCO_3$ growth, the Ur multilayer thin film, which was ~45 nm in thickness, was quite smooth, as shown in Figure 2a. After 2 min of the treatment of the multilayer film in a crystal-forming aqueous solution, droplet-shaped ACC particles were sporadically formed from the Ur multilayer surface, and the surface coverage of ACC particles was ~34%, as shown in Figure 2b. The diameter of ACC droplets varies from 50 nm to 200 nm, and the height of the ACC droplets is ~170 nm. As the growth time (or treatment time) lapses, the lateral size of ACC droplets increases to ~400 nm (see Figure 2c) and the empty space between the growing ACC droplets is also covered with newly initiated ACC droplets. Thus, the surface coverage increases up to 73%. After 10 min of treatment of the multilayer surface, the entire surface of the Ur multilayer is fully covered with the ACC droplets, showing a turtleshell-like morphology shown in Figure 2d. We also noted that a thick ACC film of ~400 nm was successfully formed on the Ur multilayer by merging neighboring ACC droplets on the surface (the root-mean-square (rms) roughness of the ACC thin film is 29 ± 1.4 nm, as measured by atomic force microscopy (AFM)).

Several studies have previously addressed on the formation of $CaCO_3$ thin films accompanied by the slow

(43) Choi, S.-J.; Yoo, P. J.; Baek, S. J.; Kim, T. W.; Lee, H. H. *J. Am. Chem. Soc.* **2004**, *126*(25), 7744.

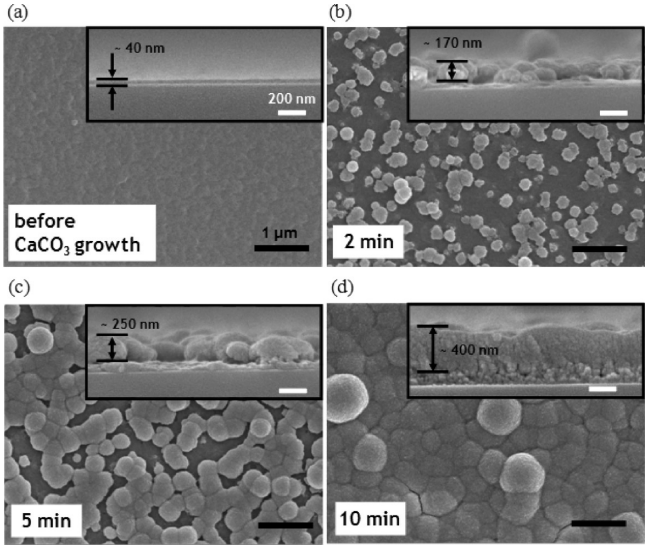

Figure 2. FE-SEM images of Ur multilayers: (a) before the onset of $CaCO_3$ growth and after (b) 2, (c) 5, and (d) 10 min of $CaCO_3$ growth. The inset in each figure represents the cross-sectional FE-SEM image of the sample. The concentrations of $CaCl_2 \cdot 2H_2O$, urea, and $NaHCO_3$ were fixed at 0.5 M, 0.5 M, and 10 mM, respectively.

increase in CO_3^{2-} concentration through the CO_2 diffusion method.[22,24,44,45] In contrast, we note that $CaCO_3$ supersaturated solution is necessary at the onset of ACC droplet formation in the present study. As soon as the Ur multilayer film is dipped into the $CaCO_3$-forming solution, the enzymatic reaction immediately starts from the urease-immobilized multilayer surface. Carbonate ions, generated by the enzymatic reaction of urea in the solution with urease immobilized in the film, diffuse out of the multilayer surface, making the local concentration of carbonate ion (CO_3^{2-}) near the surface higher than the concentration in bulk. The small increase in carbonation ions close to the surface is enough to initiate the formation of ACC droplets on the multilayer surface. However, we also note that it is difficult to initiate the formation of ACC droplets from the surface when the crystal-forming solution is not fully saturated by $CaCO_3$ at the initial stage of growth. To investigate the effect of $CaCO_3$ supersaturation in bulk solution on the ACC nucleation on the Ur-multilayer surface, the concentration of $NaHCO_3$ was varied from 0 mM to 100 mM while the other concentrations of $CaCl_2$ and urea were all fixed at 0.5 M and 0.5 M, respectively (see Figure S2 in the Supporting Information). Without $NaHCO_3$ in the crystal-forming solution, the surface nucleation of ACC droplets was not observed at all, with only bulk $CaCO_3$ particles found. When 1 mM of $NaHCO_3$ is added to the solution, a few ACC droplets start to form on the multilayer substrate coexisting with $CaCO_3$ particles formed in bulk solution, and we finally notice that the surface nucleation of ACC droplets is dominant when the concentration of $NaHCO_3$ in the bulk solution exceeds 10 mM.

(44) Nishimura, T.; Ito, T.; Yamamoto, Y.; Yoshio, M.; Kato, T. *Angew. Chem., Int. Ed.* **2008**, *47*(15), 2800.
(45) Falini, G.; Albeck, S.; Weiner, S.; Addadi, L. *Science* **1996**, *271* (5245), 67.

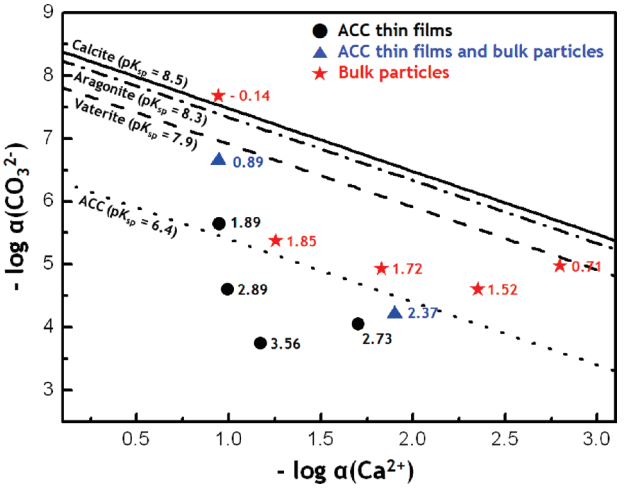

Figure 3. Formation of ACC thin films and/or bulk crystal particles on Ur multilayers: (●) ACC thin films, (▲) ACC thin films and bulk crystal particles, and (★) bulk crystal particles. The saturation index (SI) value of each crystal-forming solution is given beside each symbol in the plot. Different straight lines illustrate the solubility product (K_{sp}) values of different $CaCO_3$ polymorphs (the pK_{sp} values for calcite, aragonite, vaterite, and ACC are 8.5, 8.3, 7.9, and 6.4, respectively).

Furthermore, we varied the concentrations of both $CaCl_2$ and $NaHCO_3$ to investigate the critical saturation index of $CaCO_3$ solution for the formation of ACC thin films (see Figure 3). The concentrations of $CaCl_2 \cdot 2H_2O$ and $NaHCO_3$ were varied from 0.1 mM to 0.5 M with random combinations. The saturation index of a crystal-forming solution is calculated by the equation given below:

$$\text{Saturation Index (SI)} = \log \text{IAP} - \log K_{sp}$$

where IAP is the ion activity product in a crystal-forming solution (IAP = $\alpha'(Ca^{2+})\alpha'(CO_3^{2-})$, and K_{sp} is the solubility product of various $CaCO_3$ crystal polymorphs ($K_{sp} = \alpha(Ca^{2+})\alpha(CO_3^{2-})$. The negative logarithmic K_{sp} values (pK_{sp}) of calcite, aragonite, vaterite, and ACC are 8.5, 8.3, 7.9, and 6.4, respectively, and these pK_{sp} values for different crystal polymorphs are plotted as straight lines, as shown in Figure 3. The formation of ACC thin films, bulk crystal particles, or both in each experimental set is marked by different symbols (filled circles: ACC thin films; filled triangles: ACC thin films and bulk particles; filled stars: bulk particles) in the plot of minus log CO_3^{2-} activity ($-\log \alpha(CO_3^{2-})$) versus minus log Ca^{2+} activity ($-\log \alpha(Ca^{2+})$), where ion activities are calculated by Visual MINTEQ. From the equation shown above, the SI value of each crystal-forming solution, which is the number given beside each symbol in Figure 3, is obtained based on the K_{sp} value of calcite crystals (pK_{sp} = 8.5). When the SI value of crystal-forming solutions is lower than 1.85, bulk crystal particles are dominantly produced in comparison with an ACC thin film on the multilayer surface. However, in the case of relatively high SI values (> 1.89), ACC thin films were mainly formed on Ur multilayers without $CaCO_3$ crystal particles in bulk solution. Remember here that the calculated SI values indicate the initial conditions of the growth solution, not during the ACC film formation.

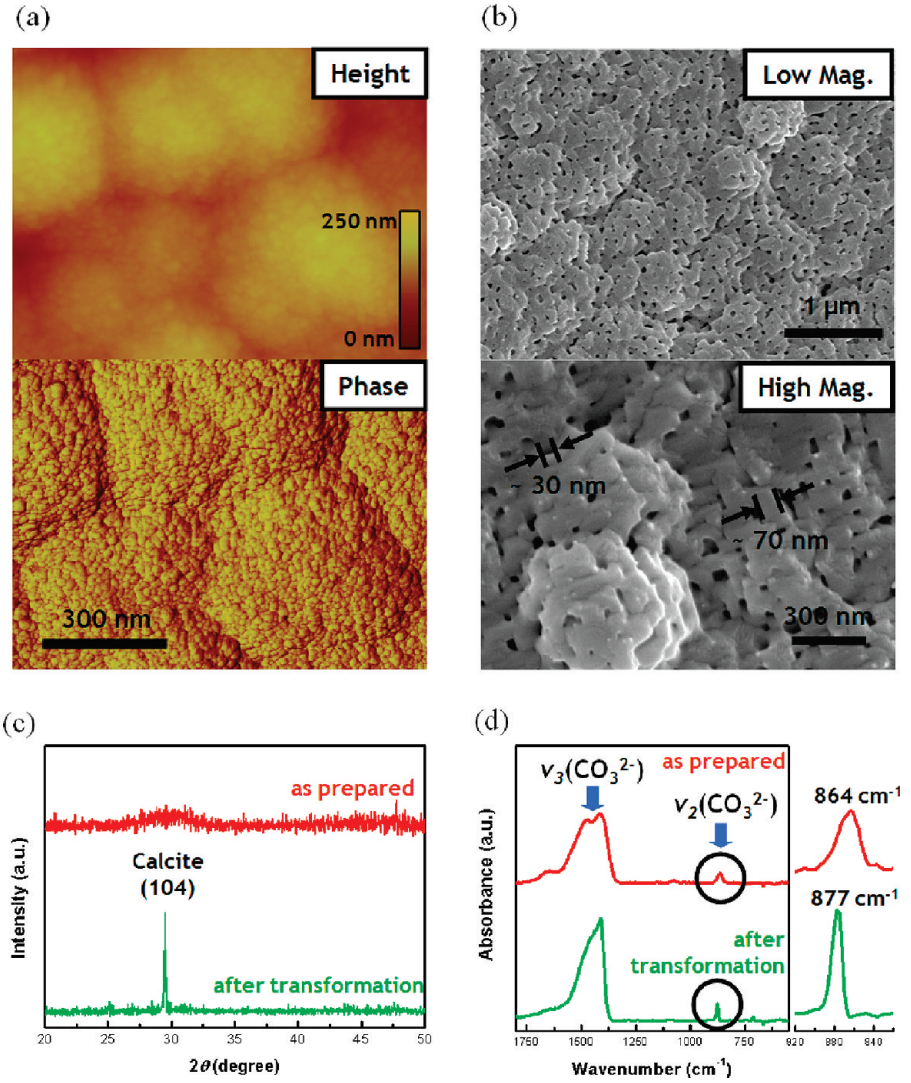

Figure 4. (a) AFM images of an ACC thin film grown on a Ur multilayer for 10 min; (b) FE-SEM images (for both low and high magnifications) of a NCC thin film after the phase transformation at 58% humidity overnight; (c) XRD data and (d) FT-IR spectra on both of the prepared ACC and NCC thin films are also shown.

The surface morphology of ACC thin films is investigated by atomic force microscopy (AFM) (see Figure 4a). As shown in the height image of Figure 4a, the surface of an ACC thin film consists of bumpy hills, in good agreement with the FE-SEM image of Figure 2d. In addition, the phase image of Figure 4a shows that a single ACC droplet ~300 nm in size is formed by the aggregation of ACC nanoparticles ~8 nm in size. After the phase transformation under 58% humidity,[46] the initial bumpy surface structure of ACC droplets is converted to a honeycomb-like nanoporous structure, which is confirmed to be the assembled structure of (104)-faceted calcite nanocrystals (see Figure 4b). The pore size is ~30 nm, and the width of honeycomb-like frame is ~70−150 nm. The crystal structure of such a nanostructured $CaCO_3$ (NCC) thin film was examined by X-ray diffraction (XRD) analysis (see Figure 4c). After the phase transformation, a strong (104) peak of calcites is observed, implying that the "honeycomb-shaped" nanocrystalline phases are oriented along the (104) plane. In the case of the "as prepared" ACC sample, the lack of sharp peaks in the XRD pattern confirms the amorphous state of $CaCO_3$. In the Fourier transform infrared (FT-IR) spectra shown in Figure 4d, a broad vibronic peak at 864 cm^{-1}, which is attributed to carbonate out-of-plane bending (ν_2), and two split peaks at 1472 cm^{-1} and 1417 cm^{-1} (ν_3) appear, confirming the ACC formation.[9,24] In the case of the NCC thin film, a sharp peak at 877 cm^{-1} (ν_2), as well as a single peak at 1411 cm^{-1} (ν_3), indicates the formation of calcite crystals after the phase transformation, under controlled humidity.

Previous studies have reported that the transformation from an ACC thin film to a crystalline thin film is accompanied by the volume contraction caused by the elimination of water molecules during the transformation, generating irregularly shaped pores with a rough surface.[46,47] However, the present study demonstrates that the regular honeycomb-shaped nanoporous structure was obtained after the phase transformation. We

(46) Xu, X.; Han, J. T.; Kim, D. H.; Cho, K. *J. Phys. Chem. B* **2006**, *110* (6), 2764.

(47) Volkmer, D.; Harms, M.; Gower, L.; Ziegler, A. *Angew. Chem., Int. Ed.* **2005**, *44*(4), 639.

assumed that the morphological change from ACC to NCC crystals is caused by the mobility of ACC, which can be tuned using relative humidity to control the amount of water absorbed in the ACC.[46] To verify the effect of ACC mobility on the morphological change during the phase transformation to NCC crystals, the relative humidity in a closed chamber was varied from 58% up to 100% (see Figure S3 in the Supporting Information). In the case where the ACC substrate was treated in 100% humidity, the ACC droplets become highly mobile and readily aggregate with each other, resulting in the formation of micrometer-sized bulk crystals with 9.8% surface porosity, based on the image analysis of FE-SEM plan-view images of porous films. As the relative humidity is decreased to 75% and 58%, we note that the crystal size of transformed NCCs decreases, resulting in a gradual reduction in surface porosity, to 6.6% and 4.7%, respectively. In the case of a treatment with 58% humidity, the size of NCC crystals is limited to several hundred nanometers, presumably because of the limited mobility of ACC droplets during the crystallization, resulting in the honeycomb-shaped nanoporous thin films. In addition, we think that a small amount of polyelectrolytes (PDAC) captured in the ACC droplets could also be one of the reasons influencing the formation of unique morphologies in the NCC thin films.[48,49] The content of polymeric impurities was estimated to be ~1.3 at. % nitrogen, calculated from X-ray photoelectron spectroscopy (XPS). (See Figure S4 in the Supporting Information.)

This novel synthetic route to obtain NCC thin films allow us to realize NCC thin films in two-dimensional patterns as well as three-dimenional complex structures, taking full advantage of the conformal coating capability of the layer-by-layer deposition, based on urease.[50] Figure 5a shows the FE-SEM image of two-dimensional $CaCO_3$ crystal thin film patterns, fabricated by the initial formation of a surface-nucleated ACC film on a patterned photoresist (PR) surface, the phase transformation into a NCC crystal thin film, and the final PR liftoff, following the same fabrication procedure for the patterning of layer-by-layer multilayer films developed in our research group.[51] High-integrity two-dimensional $CaCO_3$ crystal thin-film patterns are obtained and the crystalline nanostructure is also well-inscribed into the patterned area, as shown in the inset of Figure 5a. Three-dimesional micrometer-sized structures, such as polystyrene (PS) microbeads (2 μm in diameter) and a sawtooth-shaped micropatterned polyurethane substrate, were also used as templating substrates for the NCC crystal film growth. We observe that the PS microbeads are completely covered, with NCC crystal thin films showing the "honeycomb" morphology on a curved surface (see Figure 5b). We note that the increase in the diameter of NCC-coated PS microbeads is ~1 μm, indicating that ~500-nm-thick NCC crystals form at the PS surface. Figure 5c shows the sawtooth-shaped micropatterned polyurethane (with a pitch of 20 μm) coated with a NCC crystal thin film. The low-magnification picture (shown as the inset in Figure 5c) verifies that the uniform coating of a NCC crystal thin film can be realized over a large area. We have clearly demonstrated that uniform $CaCO_3$ crystal thin films can be grown and patterned on any shape of substrates as far as the substrates are coated with uniform multilayers that contain immobilized urease prepared via layer-by-layer deposition.

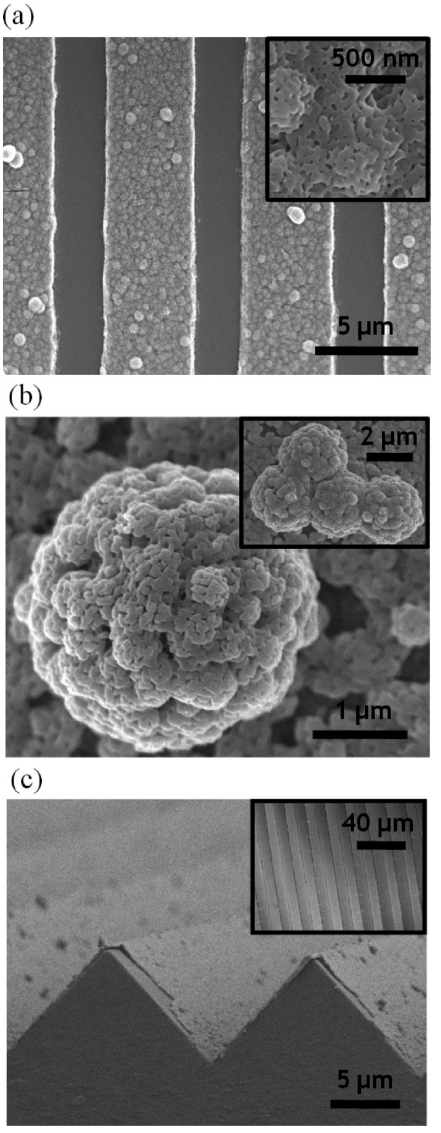

Figure 5. (a) FE-SEM image of a NCC thin film in two-dimensional line patterns (width of 5 μm and pitch of 7 μm) prepared by the $CaCO_3$ growth on photoresist (PR) patterns, followed by lifting off the PR film; a high-magnification image of the NCC thin film is also shown in the inset. (b) FE-SEM image of NCC thin films formed on polystyrene beads 2 μm in diameter; the inset picture shows four PS beads coated with NCC thin films in low magnification. (c) Sawtooth-shaped polyurethane micropatterns coated with a NCC thin film are shown in the tilted-sectional FE-SEM view; a plan-view image of the same pattern is also shown in the inset.

Conclusions

Honeycomb-shaped nanostructured $CaCO_3$ thin films were synthesized through the phase transformation of

(48) Colfen, H.; Antonietti, M. *Langmuir* **1998**, *14*(3), 582.
(49) Rautaray, D.; Sainkar, S. R.; Sastry, M. *Chem. Mater.* **2003**, *15* (14), 2809.
(50) Caruso, F.; Caruso, R. A.; Mohwald, H. *Science* **1998**, *282*(5391), 1111.
(51) Cho, J.; Jang, H.; Yeom, B.; Kim, H.; Kim, R.; Kim, S.; Char, K.; Caruso, F. *Langmuir* **2006**, *22*(3), 1356.

ACC thin films, which is produced by the enzymatic reaction of urease multilayers deposited on a substrate by the layer-by-layer method. We have also shown that the ACC thin films can be realized on a large substrate under controlled experimental conditions, and the ACC thin films can be readily transformed to porous crystalline thin films assembled in {104}-faceted calcite nanocrystals. This synthetic strategy to form NCC thin films was extended to the NCC thin films with two-dimensional line patterns and even formed on the surfaces of three-dimensional microstructures. We believe that this new synthetic scheme to obtain biomineral thin films, combined with flexible processing methods (i.e., layer-by-layer deposition), could cast fresh insight into the manufacturing of biomineral thin films on synthetic substrates, in terms of nanostructure control and large-area fabrications for further applications. One example would be such that the NCC thin films could be a potential candidate to improve efficiency and capacity in eliminating hazardous heavy metals such as Pb and Cd ions in polluted water, taking full advantage of the large surface area of nanostructured thin films, as well-documented in recent studies.[52,53]

(52) Godelitsas, A.; Astilleros, J. M.; Hallam, K.; Harissopoulos, S.; Putnis, A. *Environ. Sci. Technol.* **2003**, *37*(15), 3351.
(53) Kohler, S. J.; Cubillas, P.; Rodriguez-Blanco, J. D.; Bauer, C.; Prieto, M. *Environ. Sci. Technol.* **2007**, *41*(1), 112.

Acknowledgment. This work was financially supported by the Korea Science and Engineering Foundation (KOSEF) grant, through the Acceleration Research Program (R17-2007-059-01000-0) and the NANO Systems Institute-National Core Research Center (R15-2003-032-02002-0) funded by the Ministry of Education, Science and Technology (MEST) of Korea. We also acknowledge the financial support from the MEST on graduate programs at Seoul National University through the Brain Korea 21 Program and the World Class University (WCU) Program of Chemical Convergence for Energy and Environment (C2E2; 400-2008-0230). We are also grateful to Hyo Seon Suh for providing the 2D pattern and Dr. T. Kim for providing the sawtooth-shaped pattern.

Supporting Information Available: Ellipsometric thickness data, FT-IR spectra, and UV−visible absorbance data for the characterization of Ur-multilayers, OM images for ACC thin film formation (depending on the concentration of $NaHCO_3$), FE-SEM images of $CaCO_3$ films transformed with various humidity, and XPS data from the surface of ACC thin film. This material is available free of charge via the Internet at http://pubs.acs.org.